Coupling MAR (Modèle Atmosphérique Régional) with PISM (Parallel Ice Sheet Model) mitigates the positive melt–elevation feedback

Alison Delhasse, Johanna Beckmann, Christoph Kittel, Xavier Fettweis

The Cryosphere, 18, 633–651, 2024
https://doi.org/10.5194/tc-18-633-2024

The Cryosphere Open Access EGU

Coupling MAR (Modèle Atmosphérique Régional) with PISM (Parallel Ice Sheet Model) mitigates the positive melt–elevation feedback

Alison Delhasse[1], **Johanna Beckmann**[2,3], **Christoph Kittel**[4,1], **and Xavier Fettweis**[1]

[1]Department of Geography, Laboratory of Climatology, SPHERES, University of Liège, Liège, Belgium
[2]Potsdam-Institut für Klimafolgenforschung (PIK), Member of the Leibniz Association, Potsdam, Germany
[3]Securing Antarctica's Environmental Future, Monash University, School of Earth,
Atmosphere and Environment, Clayton, Australia
[4]Institut des Géosciences de l'Environnement (IGE), Université Grenoble Alpes, CNRS, IRD, G-INP, Grenoble, France

Correspondence: Alison Delhasse (alison.delhasse@uliege.be)

Received: 1 February 2023 – Discussion started: 15 February 2023
Revised: 2 November 2023 – Accepted: 27 November 2023 – Published: 12 February 2024

Abstract. The Greenland Ice Sheet is a key contributor to sea level rise. By melting, the ice sheet thins, inducing higher surface melt due to lower surface elevations, accelerating the melt coming from global warming. This process is called the melt–elevation feedback and can be considered by using two types of models: either (1) atmospheric models, which can represent the surface mass balance (SMB), or SMB estimates resulting from simpler models such as positive degree day models or (2) ice sheet models representing the surface elevation evolution. The latter ones do not represent the surface mass balance explicitly as well as polar-oriented climate models. A new coupling between the MAR (Modèle Atmosphérique Régional) regional climate model and the PISM (Parallel Ice Sheet Model) ice sheet model is presented here following the CESM2 (Community Earth System Model; SSP5-8.5, Shared Socioeconomic Pathway) scenario until 2100 at the MAR lateral boundaries. The coupling is extended to 2200 with a stabilised climate ($+7\,^{\circ}$C compared to 1961–1990) by randomly sampling the last 10 years of CESM2 to force MAR and reaches a sea level rise contribution of 64 cm. The fully coupled simulation is compared to a one-way experiment where surface topography remains fixed in MAR. However, the surface mass balance is corrected for the melt–elevation feedback when interpolated on the PISM grid by using surface mass balance vertical gradients as a function of local elevation variations (offline correction). This method is often used to represent the melt–elevation feedback and prevents a coupling which is too expensive in computation time. In the fully coupled MAR simulation, the ice sheet morphology evolution (changing slope and reducing the orographic barrier) induces changes in local atmospheric patterns. More specifically, wind regimes are modified, as well as temperature lapse rates, influencing the melt rate through modification of sensible heat fluxes at the ice sheet margins. We highlight mitigation of the melt lapse rate on the margins by modifying the surface morphology. The lapse rates considered by the offline correction are no longer valid at the ice sheet margins. If used (one-way simulation), this correction implies an overestimation of the sea level rise contribution of 2.5 %. The mitigation of the melt lapse rate on the margins can only be corrected by using a full coupling between an ice sheet model and an atmospheric model.

1 Introduction

The mass balance (MB) of the Greenland Ice Sheet (GrIS) is a key factor of the future estimation of sea level rise (SLR) (Oppenheimer et al., 2019). Within the components of the GrIS MB, changes in surface mass balance (SMB) and iceberg discharge, surface meltwater runoff appears to be the main contributor to future SLR (Goelzer et al., 2013, 2020; Enderlin et al., 2014; Choi et al., 2021).

As a long-term consequence, the ongoing ice melt will result in a reduction in the ice sheet topography. Such a thinning will influence the regional atmospheric circulation, particularly affecting the spatial distribution of precipitation (Vizcaíno et al., 2010). Moreover, it will amplify surface melting through a positive feedback, since the lower ice sheet elevation results in intensified warming and increased melting (hereafter, melt–elevation feedback). Changes in topography are generally not considered in climate models, but they are in ice sheet models (ISMs). Conversely, atmospheric models, particularly regional climate models (RCMs), can represent the SMB and its components in a more realistic way than ISMs by explicitly resolving the physical polar processes involved in interactions between the atmosphere and ice or snow surfaces. Therefore, the most optimal method to represent the melt–elevation feedback would involve coupling an RCM with an ISM.

Yet, this kind of coupling presents two main challenges. First, an RCM–ISM coupling is nontrivial due to disparities in spatial and temporal scales between the two model types. Simulations of ice flow processes require relatively large time steps (on the order of 1 month), in contrast to atmospheric dynamic resolution (on the order of 1 min), which is significantly shorter. Conversely, ISMs are implemented on a finer grid (on the order of 1 km) compared to RCMs (on the order of 10 km). These differences result in extended computational times for coupled simulations. Furthermore, depending on the specific ISM used in an RCM–ISM coupling, the response to climate change may significantly vary (Goelzer et al., 2013, 2020), while RCMs tend to simulate a relatively similar SMB for the same large-scale forcing (Fettweis et al., 2020). This implies the necessity of multiple couplings with several ISMs and RCMs to accurately quantify uncertainties.

An often-used alternative to coupling is to impose atmospheric conditions from an RCM onto an ISM. In such cases, either the ISM calculates SMB based on the monthly mean temperature change (Robinson et al., 2011) or the SMB is directly imposed on the ISM (Goelzer et al., 2013). However, as the topography and ice mask remain fixed in the RCM, this fails to account for the positive feedback between melt and elevation. In this context, it is possible to employ vertical gradients as a function of local elevation variations (implicitly considering the melt–elevation feedback) to correct the elevation-dependent outputs generated by the RCM for topographic variations simulated by the ISM (Franco et al., 2012; Helsen et al., 2012). Subsequently, ISMs can employ the corrected outputs from the RCM as direct inputs. This offline method has notably been employed in the Ice Sheet Model Intercomparison Project (ISMIP6; Goelzer et al., 2020) for the Coupled Model Intercomparison Project Phase 6 (CMIP6) exercise. The use of an offline correction is effective as long as SMB (especially melt) is predominantly influenced by surface elevation changes through the temperature lapse rate. However, its effectiveness may diminish when surface elevation changes start to impact synoptic circulation patterns, leading to alterations in precipitation patterns, for example. Both approaches were compared in Le clec'h et al. (2019) using the GRISLI (Grenoble Ice Sheet and Land Ice; an ISM) and MAR (Modèle Atmosphérique Régional; an RCM) models, driven by MIROC5 (Model for Interdisciplinary Research on Climate; from CMIP5). The study underscored the need for coupling beyond 2100 due to the melt–elevation feedback and precipitation–circulation changes that cannot be accurately represented when using a simple offline correction, especially as topographic changes become increasingly substantial.

Given that the coupling depends on the chosen ISM, we introduce a new coupling between the MAR climate model and the Parallel Ice Sheet Model (PISM), following an extremely warm scenario (CESM2, Community Earth System Model; SSP5-8.5, Shared Socioeconomic Pathway) until 2200. This coupling explicitly accounts for the melt–elevation feedback and is compared against an alternative offline correction method for SMB. We have three main objectives: (1) to analyse the evolution of the GrIS until 2200 under an extreme scenario using this new coupling, (2) to evaluate the ability of the offline method to represent the melt–elevation feedback by comparing our coupled simulation with the one-way experiment, and (3) to elucidate which atmospheric feedback mechanisms and physical processes are influenced by changes in surface topography.

Section 2 describes the methodology and different experiments used in the study. The first part of the result in Sect. 3.1 presents the GrIS evolution as simulated with our coupling until 2200. Section 3.2 compares one-way and two-way experiments by evidencing new negative feedback triggered by the evolving surface topography of the GrIS in the two-way coupling method. Results are discussed in Sect. 4, and we end with the conclusion in Sect. 5.

2 Data and methodology

2.1 Models

2.1.1 MAR regional climate model

The MAR model is a hydrostatic regional climate model specially designed to represent polar climates. It is widely utilised over Greenland (Delhasse et al., 2020; Fettweis et al., 2020, 2021; Hofer et al., 2020) and extends its application to Antarctica as well (Agosta et al., 2019; Kittel et al., 2021; Amory et al., 2021). Version 3.11.5 of MAR (MAR hereafter; Fettweis et al., 2021) is used here at a spatial resolution of 25 km. For the coupling process, the important variables are SMB and surface temperature (ST), which are required as inputs to the ISM. These surface variables originate from the interactions between the atmosphere and the first snow/ice layers of the ice sheet, which are represented by the Soil

Ice Snow Vegetation Atmosphere Transfer (SISVAT) module within MAR. The ability of MAR in simulating atmosphere–ice interactions, particularly near-surface temperature (Delhasse et al., 2020), plays a key role in the successful coupling, as it determines the two input variables required by the ISM (SMB and ST). Note that the MAR evaluation mentioned here is based on a version of MAR at a spatial resolution of 15 km (Delhasse et al., 2020).

As MAR is a regional climate model, it necessitates lateral forcing fields every 6 h to accurately represent its own climate within the chosen domain. Therefore, we selected one of the most climate-sensitive models (Hofer et al., 2020) from the CMIP6 model ensemble (CESM2) using the SSP5-8.5 scenario as outlined by the Intergovernmental Panel on Climate Change (IPCC; Eyring et al., 2016; O'Neill et al., 2016; Riahi et al., 2017), which was available at the outset of our study. The equilibrium climate sensitivity (a hypothetical value of global warming at equilibrium for a doubling of atmospheric CO_2 concentration relative to a 140-year period in the pre-industrial era) of CESM2 is $+5.2\,^{\circ}\mathrm{C}$ (mean of CMIP6: $+3.2\,^{\circ}\mathrm{C}$, Meehl et al., 2020). This choice was motivated by our intention to represent the most extreme (i.e. warmer) future scenario for the GrIS. SSP5-8.5 represents the most extreme scenario with an additional radiative forcing of $8.5\,\mathrm{W\,m^{-2}}$ projected for 2100. The aim is to highlight the limitations of both methods in representing the melt–elevation feedback under conditions of extreme warming.

CESM2 (SSP5-8.5, 6 h outputs) is currently only available until 2100. To extend our simulations up to 2200, we force MAR with the last 10 years (2091–2100) of CESM2 data, randomly sampled across the period of 2101–2200 (Table S1 in the Supplement). This means we apply a stabilised climate (mean conditions and interannual variability) to Greenland over 100 years. This extension of the large-scale forcing enables us to distinguish the effect of the rapidly increased warming projected with this scenario until 2100 compared to the effect of continued stable warming of $+7\,^{\circ}\mathrm{C}$ above Greenland until 2200.

The polar version of MAR requires a fairly long spin-up period to reach an equilibrium state for both the snowpack and the atmosphere. Concerning the snowpack, the parameters that are important for achieving an equilibrium state and representing a coherent configuration (temperature, density and liquid water content, Lefebre et al., 2003) are pre-initialised based on former simulations. These simulations have undergone an extensive spin-up process spanning over 50 years to establish a coherent representation of the snowpack (Fettweis et al., 2020).

2.1.2 PISM ice sheet model

To represent the dynamics and surface elevation of the Greenland Ice Sheet (GrIS), we utilise the Parallel Ice Sheet Model (PISMv1.2.1, called PISM hereafter), a high-resolution numerical ice sheet–ice shelf model (Bueler and Brown, 2009; Winkelmann et al., 2011). In PISM, the geometry, temperature and basal strength of the ice sheet are incorporated into stress balance equations at each time step to determine the ice velocity. In some models, the full stress field is calculated by using the full Stokes equation. But this is computationally expensive. As an ice sheet can be treated as "shallow" (meaning the area of the ice sheet is far greater than its thickness), PISM employs two approximations for shallow ice sheets: the shallow-ice approximation (SIA) and the shallow-shelf approximation (SSA).

The SIA simplifies by neglecting membrane stresses, which involve along-flow stretching and compression, as well as transverse stresses, which result from lateral drag against slower ice or valley walls. The viscosity of the ice, affecting its flow velocity, is modulated by an enhancement factor E. We set $E = 3$ in our experiments, a value typically used for the GrIS (Aschwanden et al., 2013; Beckmann and Winkelmann, 2023). A typical SIA velocity profile in a cross-section shows zero velocity at the bed (frozen to the bed) and increasing velocities at the surface.

Faster flowing ice, such as ice streams, glaciers and shelves, is typically approximated using the SSA. In this case, longitudinal stretching dominates, and membrane stresses must be taken into account. The ice base is assumed to be slippery, and horizontal speed is approximately equal throughout the depth of the ice. This plug flow allows for depth averaging in the SSA equation. While SIA can be numerically solved individually in each ice column, the SSA is nonlocal, meaning the velocity of a certain grid point depends on the whole spatially distributed stress field.

PISM combines both approximations into a hybrid stress balance mode (Bueler and Brown, 2009; Aschwanden et al., 2012; Winkelmann et al., 2011). Throughout the entire domain, PISM calculates velocities for both SIA and SSA. SSA velocities result in very small velocities in the ice interior, where membrane stresses are low and basal resistance is high. They increase in regions with basal slip. The overall velocities in PISM for grounded ice are the sum of SSA velocities and SIA velocities, expressed as Eq. (1) (Winkelmann et al., 2011). This superposition method helps avoid discontinuities in the model.

$$v = v\_\mathrm{SIA} + v\_\mathrm{SSA} \tag{1}$$

Basal sliding of the ice over the bedrock introduces basal resistance. The speed of basal sliding is determined by the sliding law, typically a power law relating to the basal shear stress (τ_b) and yield stress (τ_c). We use an exponent of $q = 0.6$ in our "pseudo-plastic" sliding law (Eq. 2).

$$\tau_\mathrm{b} = -\tau_\mathrm{c}\frac{u}{u_\mathrm{threshold}^{q}|u|^{1-q}} \tag{2}$$

To determine the yield stress τ_c we use the Mohr–Coulomb criterion in PISM. The model considers basal resistance based on the hypothesis that the ice sheet rests on a till layer.

The yield stress represents the strength of this aggregate material at the base of an ice sheet. When the yield stress is lower than the driving stress ($\tau_c < \tau_d$) there is likely to be sliding, and thus faster velocities can be observed. The driving stress in turn is dependent on the ice thickness (H) and surface gradients (h_s) of the ice: $\tau_d \propto H h_s$. The thicker and steeper the ice, the higher the driving stress and most probably the ice velocity.

The properties of the till are further approximated by using material properties such as the friction angle. We vary the till friction angle linearly between 5 and 40° with respect to bedrock elevation (between −700 and 700 m), following Aschwanden et al. (2016). This variation in friction angle leads to lower friction at lower altitudes and below sea level, resulting in increased surface velocities at the margins of the ice sheet, thus improving the match of flow structure for the glaciers.

To match the present-day extent of the ice sheet, we impose a strong negative surface mass balance at the margins of the present-day Greenland ice mask. This setup allows only for ice retreat in our experiments.

We also enforce a minimum thickness of 50 m for floating ice at the calving front and utilise the von Mises calving law, which is suitable for glaciers in Greenland (Morlighem et al., 2016). The von Mises yield criterion is a widely adopted yield criterion in the fields of solid mechanics and structural analysis. Calving is predominantly influenced by stretching, and the von Mises stress is a fundamental measure for quantifying deformation and fracture. Therefore, it directly impacts the calving speed and is incorporated in PISM following Eq. (3).

$$c = ||v|| \frac{\sigma}{\sigma_{max}}, \tag{3}$$

where $||v||$ is the velocity perpendicular to the ice front, σ is the von Mises stress for ice (Morlighem et al., 2016) and σ_{max} is a threshold. If the von Mises stress is greater than the threshold, the ice front retreats ($c > ||v||$); if it is smaller, the ice front advances. PISM uses a threshold value of 1×10^6 Pa.

All other parameters are set to default values (University of Alaska Fairbanks, 2019). Our simulations do not consider bedrock deformation or changes in ice–ocean interaction, as we maintain constant submarine melt rates.

2.1.3 Initialisation of PISM

PISM is forced by yearly ST and SMB from MAR forced by CESM2. To achieve a stable spin-up state, we forced PISM with the MAR mean fields (ST and SMB) over 1961–1990, when the GrIS was close to being balanced (Fettweis et al., 2017). However, for a realistic thermodynamics representation of the ice sheet, the temperature evolution of the last glacial cycle has to be considered because the surface temperature slowly propagates down the ice column and determines the vertical ice profile of the ice sheet. The ice profile determines the ice softness and deformability, thus affecting the flow velocity of the ice.

For a glacial spin-up, we assume that the initial state of the ice sheet prior to a glacial cycle is identical to the present-day state, including ice topography and surface temperatures. Therefore, we start with a contemporary ice sheet and force it with surface temperatures corresponding to the last glacial cycle. To maintain model continuity, historic surface temperatures spanning the last 125 000 years were incorporated as climate anomalies into the present-day climatological mean (ST for 1961–1990). This approach means that temperature anomalies were zero at both 125 000 years ago and at the present day, but they varied during the glacial period. As our coupled spin-up progresses, we obtain different surface topographies that result in varying surface temperatures and, consequently, distinct climatological mean values (Sect. 2.3.1). By using these anomalies, we ensure that the assumption of equivalent glacial states before and after the glacial cycle remains valid, as the anomalies are consistently zero at those two time points.

The first model initialisation (Fig. 2) spanned 125 000 years, incorporating a scalar temperature anomaly derived from the 2D temperature mean field of 1961–1990, a period when Greenland was near a state of balance. This 2D temperature and SMB mean field were calculated by MAR using the present-day PISM topography. The historical time series (Johnson et al., 2019) includes the temperature derived from oxygen isotope records from the Greenland Ice Core Project (GRIP; Johnson et al., 2019). To optimise computational efficiency, we followed the grid refinement defined by Aschwanden et al. (2016). Starting in SIA-only mode and with an 18 km grid at −125 000 years, we refined our grid to 9 km at −25 000 years and to 4.5 km at −5000 years. For the last −1000 years, we maintained a fixed resolution but introduced SSA to the SIA stress regime to represent the behaviour of fast-flowing outlet glaciers. Note that the initialisation of PISM ends after the reference period 1961–1990 when the ice sheet is assumed to have been in a quasi-equilibrium.

2.2 Coupling method

The coupling between both models has been performed by exchanging yearly outputs (specifically, SMB and ST from MAR and ice thickness from PISM) on 1 January of each year from 1991 to 2200 as described in Le clec'h et al. (2019). For MAR, this induces updating the surface elevation and ice extent of the ice sheet at the beginning of each year with PISM results from the previous year, whereas SMB and ST are used as forcing fields for PISM.

Before any data exchange between the models, data have to be interpolated onto the destination grid because the two models were run at two different spatial resolutions (25 vs. 4.5 km). The surface elevation simulated by PISM is then aggregated on the MAR grid at 25 km using a

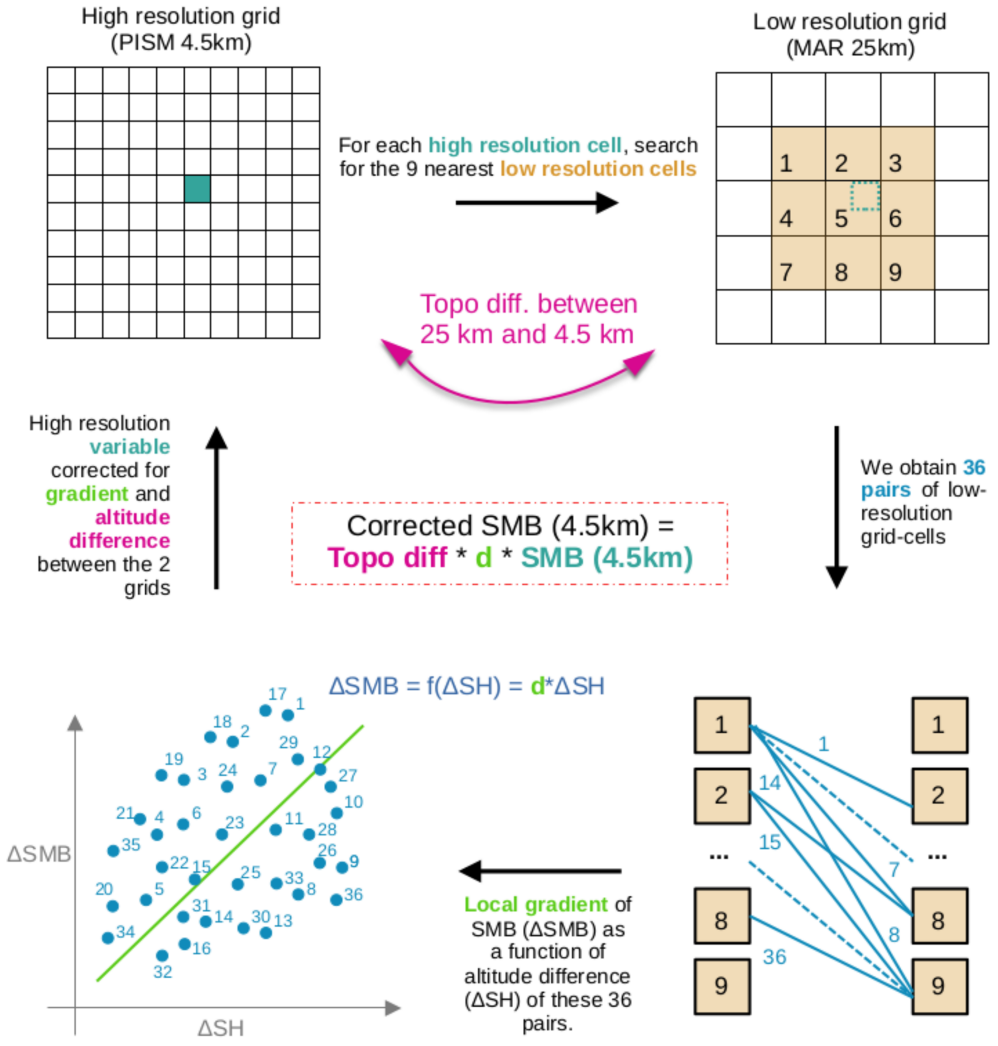

Figure 1. Steps of the offline correction as described in Franco et al. (2012). After interpolation of a variable (SMB, surface mass balance, in this figure) from a low- to higher-resolution grid, this variable is corrected to consider the influence of the temperature lapse rate with altitude. The correction is based on a local gradient (d) calculated by considering SMB differences (ΔSMB) between nine nearest low-resolution grid cells in the neighbourhood of the high-resolution grid cell position as a function of the surface elevation difference (ΔSH). Modified from Wyard (2015).

4-nearest-neighbour distance-weighted method. Conversely, MAR variables undergo interpolation onto the PISM grid at 4.5 km using the same method. However, a further correction is applied to consider the difference in altitude between the two grids at the time of interpolation thanks to local vertical SMB/ST gradients. This method is described in Franco et al. (2012) and is called offline correction hereafter.

Firstly, a linear and elevation-dependent gradient (Fig. 1) is calculated over the MAR grid, considering the values of the considered variable (for instance, SMB at 4.5 km, as illustrated in Fig. 1) of the nine surrounding grid cells of the corresponding position in the high-resolution grid. This gradient is specific to each PISM grid cell and is determined locally. An example of such a gradient is available in Fig. S1 in the Supplement. Subsequently, these gradients are utilised to correct the variable during its interpolation onto the PISM grid. The correction is performed by multiplying the interpolated variable by the gradient and the difference in surface elevation between the grid cells in MAR and in PISM. This offline correction is specifically employed to correct variables that are influenced by temperature lapse rate with altitude, namely temperature and derived variables.

2.3 Simulations

2.3.1 Initialisation of the coupling

The coupling requires initialisation to achieve an equilibrium state between the two models over a reference period (1961–1990). Successive forcings of each model by the other

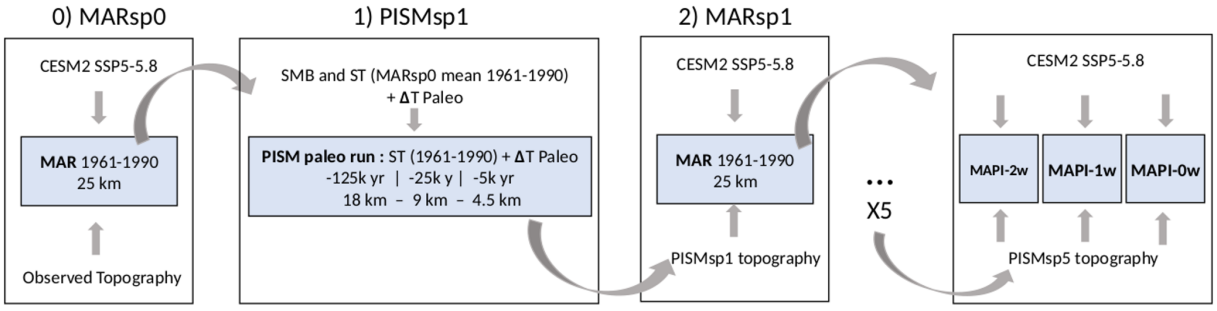

Figure 2. Steps of the coupling initialisation. Each MAR step corresponds to a 30-year-long run over the reference period (1961–1990). And each PISM step consists in a new initialisation cycle of PISM as described in Sect. 2.3.1. MAPI: coupled simulation of MAR and PISM.

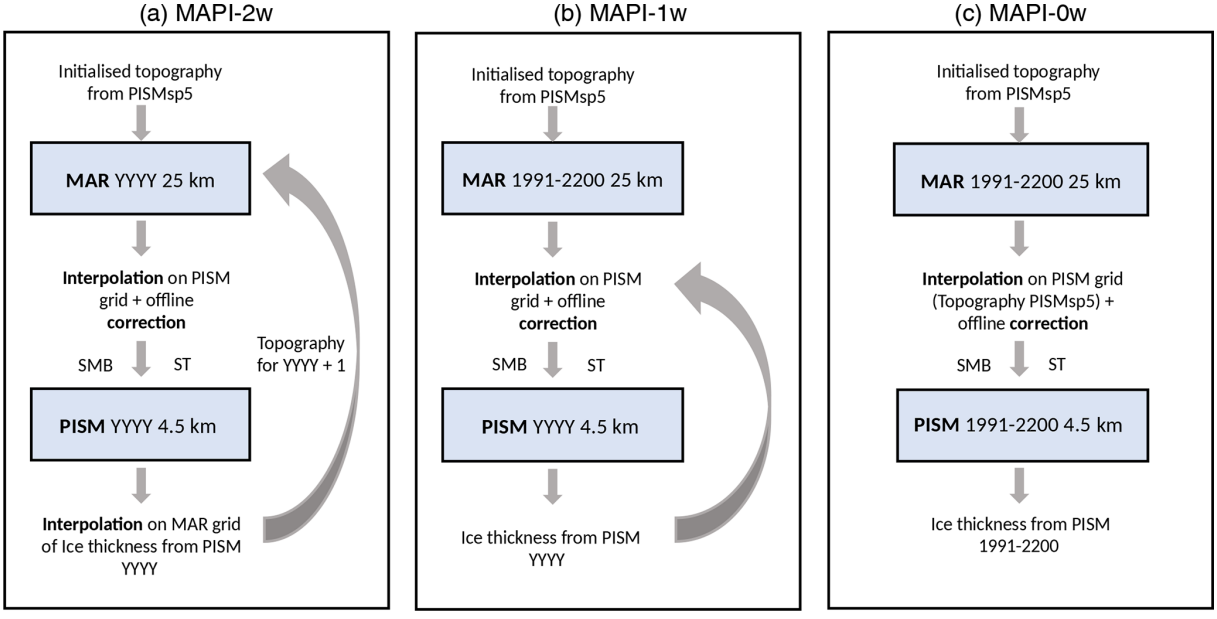

Figure 3. Coupling details for **(a)** two-way, **(b)** one-way and **(c)** zero-way experiments. YYYY is the current year of coupling.

one should produce results similar to the previous iteration over the same reference period (Fig. 2). These simulations are called spin-up hereafter. In practical terms, we firstly forced PISM using the SMB and ST climatology of MAR for 1961–1990 (MARsp0, based on the observed topography and ice mask, and CESM2 as a large-scale forcing field; Howat et al., 2014, 2017) and temperature anomalies of the last glacial cycle (see Sect. 2.1.3), resulting in a first equilibrium state (PISMsp1). This method assumes that the ice sheet topography before the last glacial cycle was similar to the pre-industrial one and reiterates this process should correct for errors in ice thickness. The next step (MARsp1) consists in running MAR using the new ice extent and topography from PISMsp1 over the same period (still 1961–1990). The corrected surface topography (PISMsp1) together with the corrected SMB and ST climatology (MARsp1) are the new base to re-start our initialisation over a whole glacial cycle, as described in Sect. 2.1.3. The new surface topography, PISMsp2, is then used to derive the new climatological mean field of 1961–1990 with MAR (MARsp2). We repeated these successive forcings (five iterations are needed here) until both models reached an equilibrium state regardless of the new forcing. This means that differences between the two spin-up stages no longer influence the other model (Fig. S2).

The PISMsp5 topography, the last step of the initialisation process, will be the initial state of the different simulations compared here and is used to run the MAR reference simulation over the reference period (MARref). As our projections could not be evaluated, we evaluated the performances of MARref over the present. To do so, we compared MAR results over the current period (1961–1990), with the initialised topography (PISMsp5) forced, on one hand, by the Earth system model used for projections (CESM2) and, on the other hand, by ERA5 reanalysis (Hersbach et al., 2020), considering observations and representing the current climate well. The main point of this evaluation is that MARref is signif-

icantly colder than MAR forced by ERA5 in the south of Greenland, but this bias does not significantly influence SMB results (see Fig. S3). It is due to the cold bias of CESM2 compared to reanalyses (Hofer et al., 2020).

The ice sheet topography and velocity field of the PISMsp5 final run and their difference to observational data sets are depicted in the Supplement (Fig. S4). The ice sheet thickness of the final spin-up is overestimated by up to 150 m in the northeast and southwest of the GrIS. In comparison, the northwest and central west are underestimated by up to 200 m compared to the observational data set (Fig. S4a). As there is no complete observational velocity data set from 1961 to 1990, we, therefore, compare it with the complete velocity data set by Joughin et al. (2018), which gives the average velocities from 1995 to 2015. Our comparison shows a general agreement of the velocity pattern with an average difference between modelled and observed ice speeds of $\pm 80\,\mathrm{m\,yr^{-1}}$ on the margins (Fig. S4b). In some fast-flowing glacier regions, differences are much larger. However, the coarse resolution (4.5 km) compared to the proximity of smaller glaciers (500 m), which are solved by the observations, lead to a strong deviation in their comparison. Furthermore, from 1995 to 2015, Greenland was not in balance, and glaciers were already experiencing speed-up and retreat (King et al., 2020).

2.3.2 Coupled simulation

The first simulation is the two-way experiment which consists in a coupled simulation of MAR and PISM called MAPI-2w hereafter. We started to run MAR in 1991 with the PISMsp5 topography forced with CESM2 (Fig. 3a). At the end of this first year, we interpolated SMB and ST on the PISM grid with the offline correction. Then, PISM is run for the same year and produces a new ice thickness that will further be aggregated onto the MAR grid to start the following year (i.e. 1992) with an updated topography. When the MAR topography is updated, we also update the ice mask in function of PISM ice extent. The melt–elevation feedback is, therefore, explicitly taken into account by the MAPI-2w simulation through an evolving topography in MAR.

2.3.3 Uncoupled simulations

The one-way experiment (called MAPI-1w hereafter) consists in a simulation where MAR is running with PISMsp5 topography (built over the reference period) for 1991–2200 without any more interaction from PISM to MAR (Fig. 3b). Then we interpolated the yearly results of SMB and ST from MAR to the PISM grid with the offline correction. Thus, the new PISM input variables were corrected for changes in the surface height of the evolving ice sheet topography of PISM compared to the fixed MAR surface elevation. The MAPI-1w experiment then considers the melt–elevation feedback a posteriori through the offline correction, meaning that it is not explicitly solved by either of the two models (MAR or PISM), nor are the implied physical processes. As MAR is evolving alone, no update on the ice mask has been done. To be consistent, we consider the smallest ice mask all along the analyses, meaning the one in 2200 of the MAPI-2w simulation, to compare both simulations.

We also consider a PISM simulation forced with fixed MAR topography corrected over the initial PISM topography (PISMsp5). This experiment is called the MAPI-0w experiment (Fig. 3c) hereafter due to its non-consideration of the melt–elevation feedback.

2.4 Representation of the results

The coupling aims to estimate the total MB of the GrIS by directly simulating the dynamical components with PISM and employing the SMB components, as simulated by MAR, as forcing for PISM.

For the sake of consistency of the results, we decided to present all results on the PISM grid, whether they are PISM or MAR outputs. The MAR variables used in the analyses below are therefore interpolated on the PISM grid. While those from the coupled simulation explicitly include the influence of the melt–elevation feedback, the variables from the uncoupled simulation (MAPI-1w) are corrected offline during the interpolation. This correction is applied to the variables dependent on the surface elevation influence, i.e. temperature, SMB, meltwater production and runoff. On the other hand, the following variables will not be corrected during their interpolation since they do not depend on the evolution of the surface elevation: total precipitation (snowfall and rainfall) and wind. However, some comparisons have been carried out on the MAR grid, but this is clearly specified each time.

The two main PISM simulations, which are compared hereafter (MAPI-2w and MAPI-1w), evolve independently and consequently have differences in surface topography. These differences are only responsible for 10 % of the MB differences between two experiments in 2200 (Fig. S6) and will be further neglected. Throughout the analysis, we will consider the MAR results interpolated on the coupled MAPI-2w PISM grid (4.5 km), regardless of whether they are from the coupled or uncoupled MAR simulation.

3 Results

3.1 Coupled MB and SMB

This section is dedicated to describing future changes in the total mass balance of the GrIS, the surface mass balance and its components compared to the reference period as simulated with the MAPI-2w coupling experiment.

Our findings indicate a rapid increase in annual mass loss under an extreme warming scenario (Fig. 4). By 2100, this corresponds to a contribution of 16 cm to sea level rise (equivalent to a total ice mass loss of more than 50×10^3 Gt)

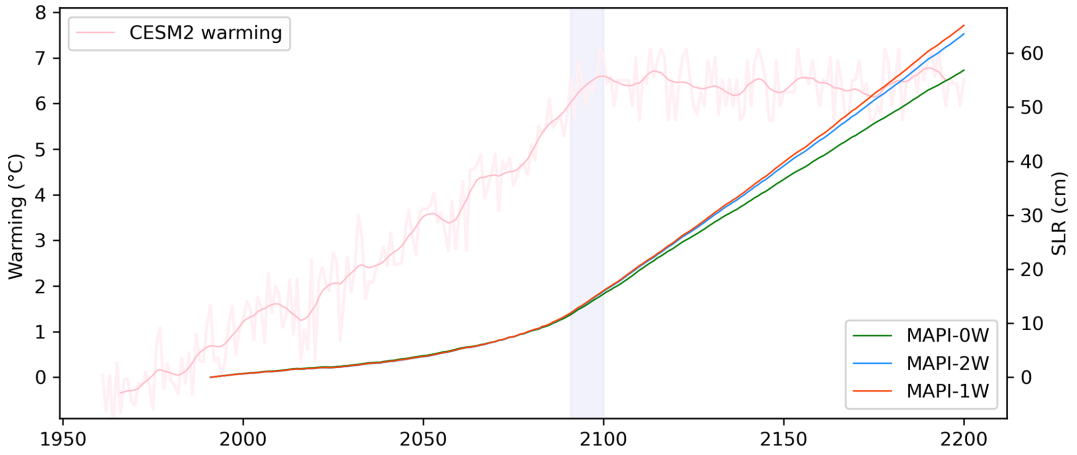

Figure 4. Contribution to sea level rise (SLR, cm) of the Greenland Ice Sheet according to MAR–PISM two-way (in blue), one-way (in red) and zero-way (in green) experiments. In pink is the corresponding warming (°C) applied in the MAR lateral boundaries following CESM2 SSP5-8.5 (mean temperature at 600 hPa over Greenland). The last 10 years of CESM2 randomly sampled until 2200 to extend the CESM2 forcing of MAR are in grey.

due to a temperature increase of +7 °C (+6.8 °C on average for 2091–2100 at 600 hPa over Greenland) compared to our reference period (1961–1990). Beyond 2100, as the temperature stabilises at +7 °C (on average for 2101–2200), the ice sheet continues to lose mass, resulting in a sea level rise contribution of 64 cm since 1991 (equivalent to a total ice mass loss of more than 200×10^3 Gt). Despite the stabilisation of warming after 2100, the mass loss continues to rise until 2200 due to earlier warming-induced acceleration before 2100.

While the GrIS is experiencing a retreat of several kilometres along its periphery (see Fig. 5), the cumulated mass balance (MB) becomes markedly negative by 2200, resulting in a decrease in surface elevation of several hundred metres along the margins of the GrIS. Notably, the western margin is particularly impacted by this mass loss and the subsequent elevation decrease. By 2200, many peripheral glaciers seem to disappear, especially in the east and north of the island.

The SMB decrease largely drives the increase in mass loss. To attribute the specific contributors to SMB loss, we examine the native 25 km output MAR-2w (Fig. 6, solid lines). The SMB evolution is characterised by a sharp decrease from 2050 to 2100, followed by a slowdown from 2100 to 2200 as the climate stabilises again. These changes in SMB are predominantly attributed to runoff (RU hereafter) resulting from increased meltwater production (ME hereafter), which does not refreeze into the snowpack.

Due to global warming, we expect higher precipitation rates, and due to the lower surface elevation, we expect especially liquid precipitation. The snowfall (SF) evolution remains constant throughout the simulation period (Fig. 6). The slight increase in total precipitation is mainly due to increased rainfall (RF). Interestingly, it is worth noting that only a small part of the RF increase (approximately 1 % when

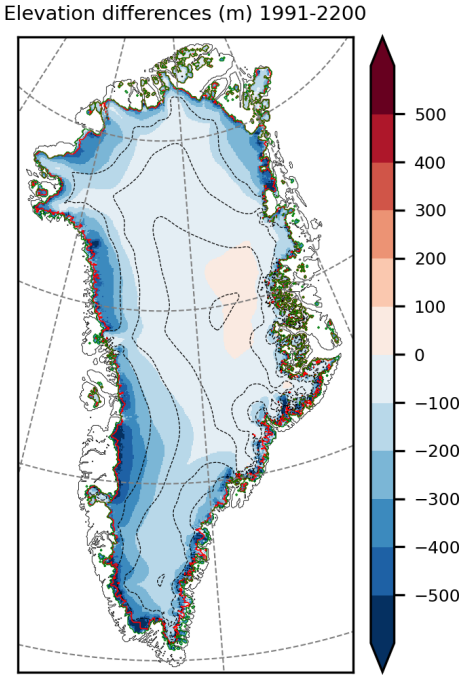

Figure 5. Surface elevation changes (m) as simulated by the two-way coupling between MAR and PISM between 1991 and 2200. In green, the ice extent is as in 1991, and in red, it is as in 2200.

comparing RF from coupled MAR in solid lines and uncoupled MAR in dashed lines) can be attributed to the reduction in surface elevation, which leads to the conversion of more SF into RF.

The spatial distribution of the SMB component changes is mainly explained by the warming scenario, emphasised by the decreasing surface elevation until 2200 (Fig. 7a). Both ME and RU (Fig. 7e and f), which drive the spatial pattern of

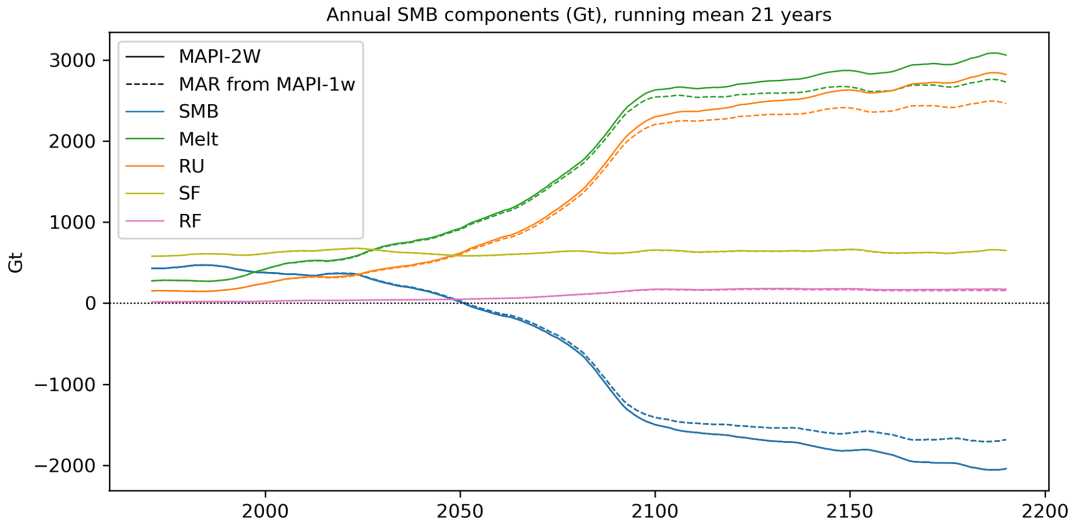

Figure 6. Surface mass balance (SMB, in blue), meltwater production (ME, in green), meltwater runoff (RU, in orange), snowfall (SF in yellow) and rainfall (RF, in pink) evolution (in Gt) as simulated by MAR–PISM two-way coupling (MAPI-2w, solid lines) from 1991 to 2200. Dotted lines are the corresponding evolution as simulated by uncoupled MAR (MAPI-1w).

the SMB (Fig. 7d), are projected to occur further inland. For instance, by 2200, almost the entire southern half of Greenland is affected by RU. This leads to a decrease in SMB in these regions, subsequently triggering changes in surface topography, evidencing the dependence of the MB on the SMB.

While total precipitation over Greenland does not change significantly (Fig. 6), its spatial distribution does change with topography compared to the reference period in the coupled simulation. There is a significant decrease in total precipitation (SF + RF, Fig. 7c) over the southeast due to synoptic features of the large-scale forcing (CESM2, not shown). Conversely, our simulation projects a significant increase over the west and north of Greenland. The westward increase can be attributed to ice sheet thinning, which allows clouds to penetrate further inland due to reduced topographic barrier effect and delayed condensation due to the further lift-up of air masses. Additionally, a synoptic pattern originating from the CESM2 forcing contributes to this precipitation increase (not shown). The changes in snowfall over the north of Greenland are attributed to higher humidity content associated with atmospheric warming, as this region is typically dry and cold under present-day conditions. This results in a slight overall increase in precipitation over the entire ice sheet, primarily due to an increase in RF resulting from global warming and surface elevation changes, as explained previously. However, these significant alterations in precipitation spatial distribution do not substantially influence the overall SMB pattern, as runoff changes outweigh them.

The reduction in mass loss from the ice sheet is accompanied by an overall speed-up of the ice dynamics further inland and a slowdown at the margins (Fig. 8a). Surface velocity is directly linked to the driving stress. Subsequently the spatial pattern of changes in driving stress (Fig. 8b) mainly explains the spatial pattern of changes in surface velocities. The driving stress depends on the product of ice thickness and surface slope. Notably, the pronounced thinning occurring at the ice sheet margins explains the reduction in driving stress in these regions. While there is also an increase in surface slope at the margins, which would typically increase the driving stress, the thinning effect holds greater significance and determines the reduction in driving stress. In contrast, although less pronounced than at the margins, the ice interior still experiences an increase in surface slope. Further inland, the amplified surface slope emphasises the driving stress, especially as the thinning is smaller than at the margins. Consequently, the increased driving stress leads to higher surface velocities.

The overall pattern of speed-up in the ice interior and slowdown at the margins is observed in both the two-way and one-way experiments. However, in MAPI-2w, ice thickness is slightly larger at the margins and thinner in the ice interior than in MAPI-1w. At the margins, this results in a reduced surface slope and, when compared to the one-way experiment, leads to slower velocities (Fig. S5b).

3.2 Comparison of coupled and uncoupled experiments

This section focuses on the differences in the results obtained from the two approaches of considering the melt–elevation feedback (MAPI-1w vs. MAPI-2w).

When comparing the total mass loss in 2200 (Fig. 4), the two strategies for representing the melt–elevation feedback (MAPI-1w vs. MAPI-2w) do not lead to significantly different total mass losses in 2200. Specifically MAPI-2w results in a total ice loss of 229×10^3 Gt, while MAPI-1w results in 234×10^3 Gt. This means that MAPI-1w overestimates the

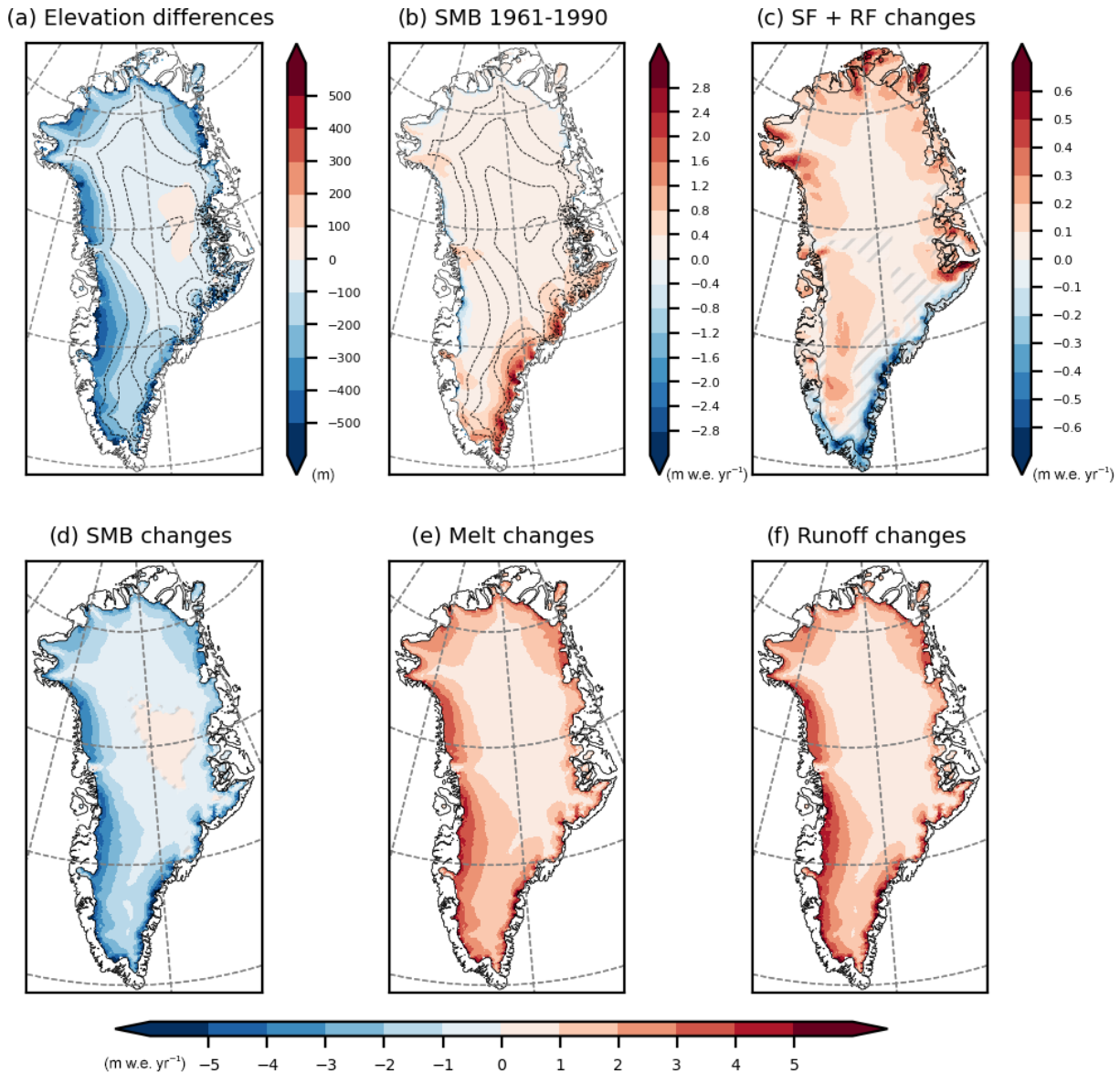

Figure 7. **(a)** Surface elevation changes (m) between 1991 and 2200 as simulated by MAR–PISM two-way coupling (MAPI-2w). **(b)** Surface mass balance (SMB, m w.e. yr^{-1}, water equivalent) for the reference period (1961–1990) as simulated by MAPI-2w. **(c)** Precipitation (snowfall, SF; rainfall, RF, m w.e. yr^{-1}), **(d)** SMB (m w.e. yr^{-1}), **(e)** meltwater production (m w.e. yr^{-1}) and **(f)** meltwater runoff (m w.e. yr^{-1}) changes in 2171–2200 compared to the reference period. Non-significant changes are hatched (smaller than the interannual variability in the reference period).

SLR contribution by 2.5 % (equivalent to 1.6 cm) compared to MAPI-2w. In contrast, MAPI-0w largely underestimates ice loss by 10.5 % (equivalent to 6.7 cm less of SLR contribution than MAPI-2w) due to its non-representation of the melt–elevation feedback. These discrepancies become more pronounced as the climate stabilises.

The overestimation of MB by MAPI-1w could be contrary to the intermediate results from MAR before interpolation and correction onto the PISM grid of both MAPI-1w and MAPI-2w simulations. If we look at these results (raw MAR outputs) before interpolation and PISM forcing, the melt rate outputs in the fully coupled mode (Fig. 6 solid lines) are higher than in the one-way coupled simulation (Fig. 6, dashed lines). However, after interpolation, when the MAR results are on the PISM grid and subsequently used to force PISM, MAPI-1w gave higher melt rates than MAPI-2w (Fig. 9a–c). This discrepancy highlights that when we apply the offline correction to correct the SMB from the melt–elevation feedback (MAPI-1w on PISM grid), the SMB becomes excessively negative compared to the two-way cou-

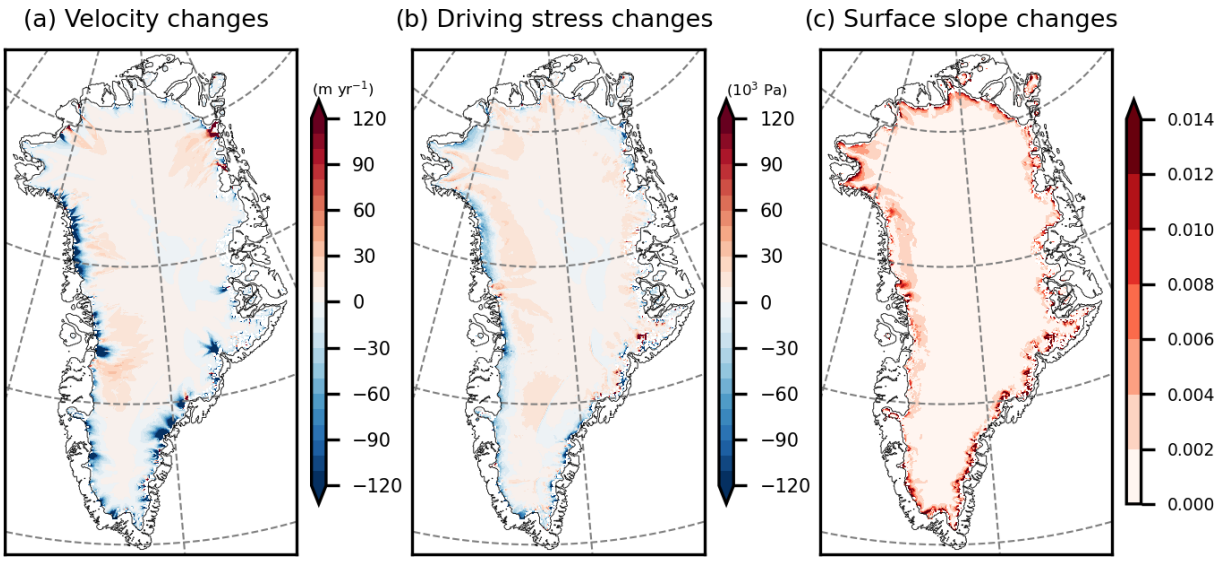

Figure 8. Changes (2200–1990) in **(a)** velocity (m yr^{-1}), **(b)** driving stress (10^3 Pa) and **(c)** surface slope of the coupled MAR–PISM simulation (MAPI-2w).

pling, which explicitly accounts for this feedback. This finding is contrary to Le clec'h et al. (2019), as discussed later in this study.

The corrected SMB provided to PISM in both MAPI-1w and MAPI-2w differs significantly at the ice sheet margin (Fig. 9a), indicating a greater mass loss for MAPI-1w. The different SMB components are analysed here (Fig. 9) to identify the cause of this underestimation in the corrected SMB for MAPI-1w. Firstly, whether on the eastern or western coast, there is a different distribution of total precipitation when simulated by MAPI-2w compared to MAPI-1w (Fig. 9f). Precipitation falls further inland (positive differences) in the coupled mode due to the flattened slope, although this difference is not significant compared to annual variability (standard deviation for 2171–2200). Therefore, this does not explain the SMB differences in the margins between the two simulations. The main driver is the meltwater runoff (Fig. 9b), resulting from the excess of ME in MAPI-1w, not refreeze in the snowpack (Fig. 9e). ME depends on sensible heat flux (SHF), which is related to air temperature and wind speed. These variables are also overestimated at the margins by MAPI-1w (Fig. 9d and e).

The underestimation of SMB in MAPI-1w is due to an overestimation of the melt–elevation feedback by the offline correction when interpolating MAPI-1w onto the PISM grid, as compared to the explicit consideration of this feedback in MAPI-2w. This correction is based on the temperature–altitude relationship to account for the melt–elevation feedback, which alters the SMB and related variables. The correction applies local linear gradients according to altitude differences between the two considered grids (MAR and PISM). We compare here, on the MAR grid, the yearly evolution of the altitude differences between the two experiments (coupled and uncoupled) with the evolution of the temperature differences. This comparison is realised in two specific locations: inside the ice sheet and on the margin (Fig. 10a). This provides an insight into the local SMB gradient as simulated by the fully coupled MAR experiment. We notice that on the margin, differences in altitude between the two MAR grids (ΔSH) explain only 61 % (69 % for melt) of the changes in temperature differences (ΔT2m and ΔME, respectively), compared to the interior of the ice sheet, where these relationships are much more dependent, with R^2 values of 0.99 and 0.94, respectively. In our example (Fig. 10a), the modifications of topography in the two-way coupling experiment have modified this linear relationship with the temperature from −0.4 °C per 100 m inside to −0.1 °C per 100 m. Similar relationships are illustrated for melt differences (Fig. 10b), confirming the modification in the linear dependence with changes in surface elevation. To further investigate this, we will compare these gradients, obtained by comparing the MAR simulations with and without changes in topography over time, with the gradients used by the offline correction. These gradients are calculated locally, taking into account the differences in altitude and in the variable considered with the surrounding grid cells. For example, for temperature, we find gradients of −0.69 and −0.65 °C per 100 m in 2200, respectively, for the same locations as in Fig. 10, inside the ice sheet and on the margins. Although these gradients have different absolute values compared to those obtained by comparing the two MAR simulations over time, the difference between the two regions is smaller. The temperature gradient applied to the margin of the ice sheet follows a dependency to the altitude similar to the gradient in the interior of the ice sheet. This explains the exaggeration of temperature and temperature-dependent variables (melt, SMB, etc.)

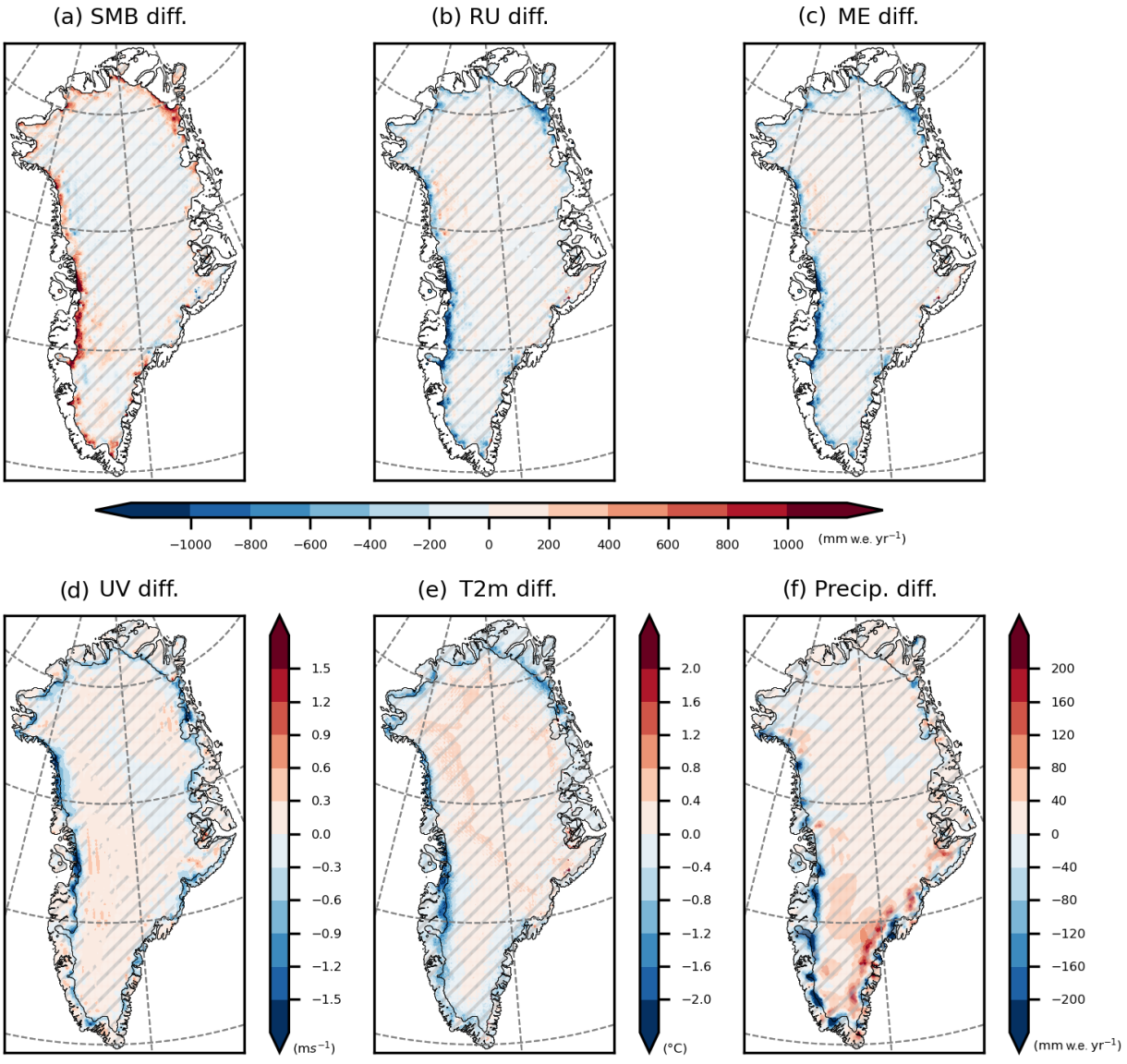

Figure 9. Differences (MAPI-2w − MAPI-1w) of **(a)** SMB (mm w.e. yr^{-1}), **(b)** runoff (RU, mm w.e. yr^{-1}), **(c)** meltwater production (ME, mm w.e. yr^{-1}), **(d)** 10 m wind speed (UV, m s^{-1}), **(e)** 2 m temperature (T2m, °C) and **(f)** total precipitation (precipitation is the sum of rainfall and snowfall) between the MAPI-2w and MAPI-1w simulations for 2171–2200. Non-significant differences are hatched (smaller than the interannual variability in 2171–2200).

on the margins by the correction. The correction uses a gradient which is too large and does not represent the processes leading to the mitigation of the temperature–altitude dependence, and, consequently, the melt–elevation feedback. Finally, we can note that beyond a 350 m drop in altitude, the association between changes in altitude and temperature (or melting) at the ice sheet margin exhibits a behaviour similar to the relationship observed within the ice sheet. Further confirmation is required through experiments involving larger elevation variations that exceed those explored in our current simulation. All these comparisons highlight two main findings: (1) the linear offline correction of SMB is no longer valid at the ice sheet margins, and (2) the changes in the linear relationship between temperature and altitude driving the melt–elevation feedback lead to mitigation of this feedback along the ice sheet margins.

The mitigation of the melt–elevation feedback in the coupled MAR simulation can be explained by the alteration of local wind and temperature patterns near the margins of the GrIS. The evolution of the topography in the coupled simulation (for instance, Fig. 11e) leads to a reduction in the melt increase with lowering elevation. In general, the production of meltwater is the result of a positive energy balance at the surface. In our study, we focus on sensible heat fluxes (SHFs),

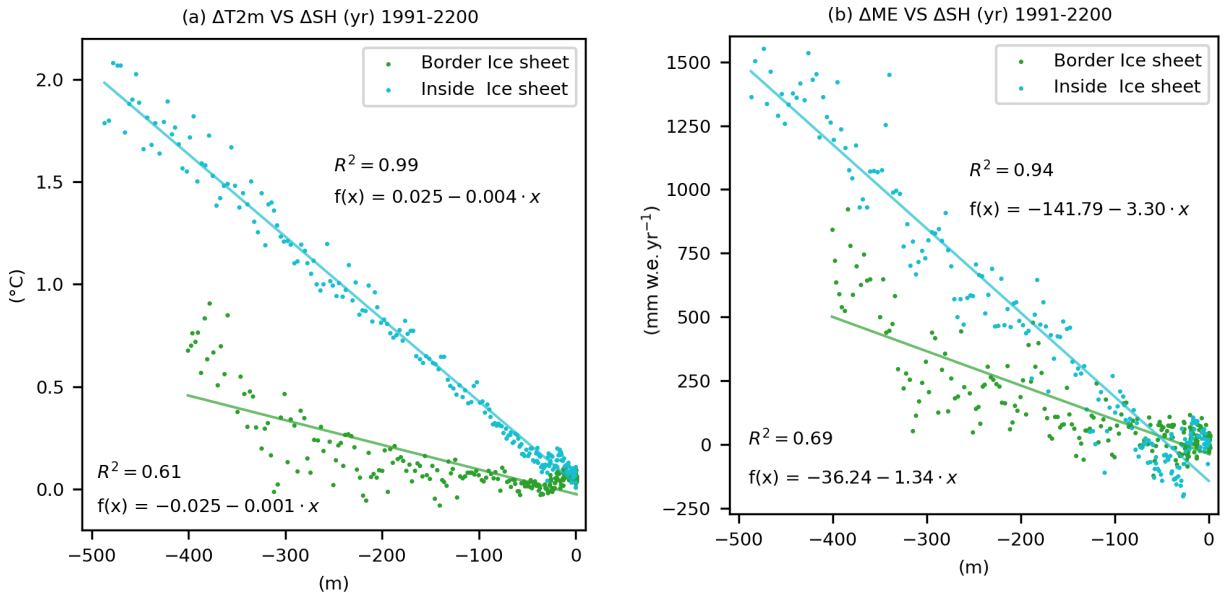

Figure 10. Association of the yearly (1991–2200) differences on MAR grid in surface elevation (ΔSH, m) with **(a)** differences in 2m temperature (ΔT2m, °C) and **(b)** meltwater production (ΔME, mm w.e. yr^{-1}) between coupled (MAPI-2w) and uncoupled (MAPI-1w) simulation for a MAR grid cell (25 km) inside the ice sheet (49.26° W, 67.05° N, in blue) and one at the boundaries with the tundra (48.83° W, 67.05° N, in green). These grid cells are located in the same section of western Greenland as in Fig. 11. Regressions are presented in the respective colours.

which are taken into account in this energy balance. An SHF is important as it depends on wind speed and temperature, both of which are influenced by alterations in topography. Therefore, we investigate here differences in these two parameters between MAPI-2w and MAPI-1w (Fig. 11b and d).

The near-surface temperature, as well as the north–south wind component, is altered along the margin, specifically in the western part of the GrIS in the fully coupled simulation. To illustrate this, we compare the vertical temperature and wind speed patterns above both simulation topographies along a transect crossing the ice sheet. The example illustrated in Fig. 11 highlights that the north–south wind component (V wind, positive northward) is larger in the uncoupled simulation on the grid cell on the ice sheet margin (inside the ice sheet, Fig. 11c and d). Furthermore, the mean near-surface temperature that appears on the 2200 topography (coupled MAR) on the same grid cell of the ice sheet margin is lower than the temperature computed on the uncoupled MAR topography while at a lower altitude (Fig. 11a and b). The changes in wind and temperature in the coupled MAR simulation provide an explanation for the reduced melt increase with lowering elevation. Note that the general wind speed, as well as west–east wind component differences, is presented in the Supplement (Fig. S7).

The temperature changes and the decrease in (V-)wind speed observed in the coupled MAR simulation, in comparison to the uncoupled one, could be explained by local modifications in the wind regime and the margin morphology. These modifications have a mitigating effect on surface melt. In general, as depicted in Fig. 11a, the uncoupled simulation exhibits a greater presence of warm air at the periphery of the ice sheet, where the original topography acts as a barrier, preventing deep air intrusion. In the coupled simulation, warm air can penetrate further inland and dissipate, resulting in an only modest increase in melting. On the other hand, in actual conditions, barrier winds occur when air masses from the tundra cross the ice sheet, which acts as an orographic barrier (Van den Broeke and Gallée, 1996). These winds induce warm-air advection from the tundra, which is warmer than the surrounding air over the ice sheet. This warm air, confined by the orographic barrier, results in northward winds along the western coast of the ice sheet, leading to high temperatures and increased wind speeds along the margins of the ice sheet. Consequently, high-melt events occur due to these high temperatures and wind speeds. As the orographic barrier weakens due to the thinning and retreat of the ice sheet (Fig. 11e) in MAPI-2w compared to MAPI-1w, the barrier winds could potentially diminish, as suggested by the decrease in V wind (south–north) in the coupled experiment. This would further result in temperature disparities between the two experiments, as less warm-air advection occurs due to the weakened barrier winds in MAPI-2w. This could impact the local gradient of melt/temperature with surface elevation and then could lead to a mitigation of melt in MAPI-2w compared to MAPI-1w, where the barrier winds remain unaffected due to unaltered topography.

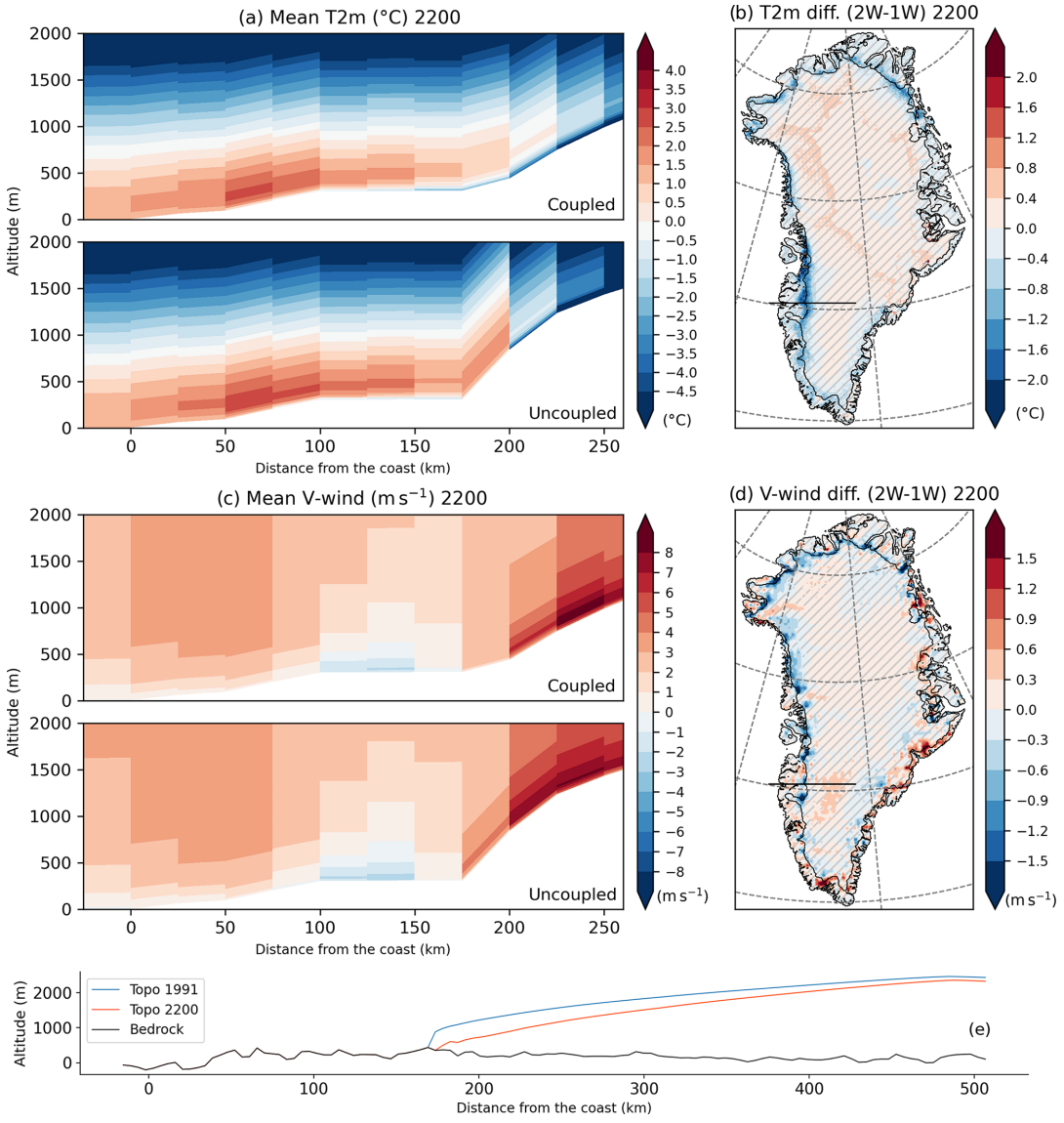

Figure 11. Cross-sections along 66.64–67.35° N of **(a)** temperature (T2m, °C) and **(c)** V wind (north–south, positive northward, m s^{-1}) on the MAR grid for the coupled (above) and the uncoupled (below) simulation. **(a, c)** The land–ice limit is situated 175 km from the coast in the MAR grid in this example. Differences in **(b)** 2 m temperature (°C) and **(d)** V wind (m s^{-1}) between two-way and one-way experiments of MAR and PISM (MAPI-2w − MAPI-1w) in 2200. Non-significant differences (lower than the interannual variability over 2171–2200) are hatched. T2m and V wind are interpolated in the PISM grid **(b, d)** to be consistent with other figures; T2m is corrected with the offline correction, but the V wind is not as it is not related to surface elevation. **(e)** Cross-section along black lines in **(b)** and **(d)** on the western coast of the PISM grid (similar to the cross-section in **a** and **c** on the MAR grid at 66.64–67.35° N) of the surface elevation (m) of MAPI-2w in 2200 (in red) and in 1991 (in blue; fixed topography in MAR for the MAPI-1w simulation), with the bedrock in black.

4 Discussion

The feedback between topography and local atmospheric circulation, as highlighted here, introduces additional uncertainty into the SLR projections. These projections are already subject to uncertainties related to ice dynamics modelling. For instance, within ISMIP6, SLR estimates for 2100 range from 6.5 to 13.5 cm under the same climate forcing conditions (MAR forced by MIROC5 using the RCP8.5 scenario), depending on the choice of ISMs and experiments (Goelzer et al., 2020). ISMIP6 experiments can be compared to our MAPI-1w simulation, as they employ a methodology that uses MAR outputs corrected offline for the melt–elevation feedback. However extending simulations using such a method could introduce uncertainties coming from the evolving topography of the ice sheet and its interaction with near-surface climate, as discussed in this study.

In a related study by Le clec'h et al. (2019), a methodology similar to ours was employed. They used MAR and the GRISLI ISM (Quiquet et al., 2012) to represent GrIS until 2150. The main difference between their study and ours, besides the ISM used, lies in the large-scale forcing field to force MAR (i.e. MIROC5, a CMIP5 model using the RCP8.5 scenario). The future climate projected by MIROC5 is less warm compared to CESM2, with a difference of approximately $+1.5\,^{\circ}\mathrm{C}$ (Hofer et al., 2020). Consequently, the SLR contributions are consequently well higher when using CESM2. For instance, the warming level projected by MIROC5 for 2100 is reached as early as 2080 in the case of CESM2. Regarding their two-way coupled simulation, given the disparity in the warming scenarios used for the coupling (MIROC5 RCP8.5 vs. CESM2 SSP5-8.5), their MB results in 2100 are similar to those of our MAPI-2w experiment in 2080. From a dynamical perspective, both studies observe a similar overall pattern of speed-up in the ice interior and slowdown at the margins of the GrIS towards the end of their respective simulations.

In contrast to Le clec'h et al. (2019), who extended their one-way simulation until 2150 using constant MAR outputs (SMB and ST), we decided to extend our MAPI-1w simulation beyond 2100 by repeating the last 10 years of large-scale forcing from CESM2 to run MAR until 2200. This was done to allow time for the snowpack to stabilise under the influence of the new, warm, stabilised climate conditions from 2101 to 2200. The main distinction between our approach and that of Le clec'h et al. (2019) is that, after 2100, our MAR simulations with a fixed topography continued to run with repeated CESM2 forcing fields. In contrast, in their corresponding simulation, MAR did not continue beyond 2100, and SMB is therefore assumed to be constant as long as the climate is stable. We compared our one-way and two-way experiment results with a simulation where the last 10 years of MAR outputs from MAPI-1w (the same 10 years as the repeated CESM2 inputs) were used directly to force PISM, extending the MAPI-1w simulation from 2100 to 2200 without running MAR any further. This approach was similar to the one used by Le clec'h et al. (2019) in their one-way experiment. It appears that in MAPI-1w, SMB continues to decrease for decades compared to the repeated fixed MAR outputs (Fig. 12). This indicates that, even without additional warming, the ablation area of the ice sheet continues to expand after 2100. The snowpack turns from an accumulation state into an ablation state over a larger portion of the ice sheet. This transition requires decades to stabilise before reaching a stable meltwater retention capacity. As demonstrated in the RetMIP exercise (Retention Model Intercomparison; Vandecrux et al., 2020), the time required to stabilise meltwater retention capacity is likely model-dependent due to parameters such as maximum liquid water retention within the snowpack and the height of the considered snowpack layer. This study also emphasises that SMB (through runoff) cannot be considered stable as soon as warming stops. During the response time of the snowpack, meltwater saturates deep layers, causing it to become warmer and denser, which reduces its capacity to retain meltwater. Once the snowpack reaches its maximum retention capacity, it transforms into impermeable firn or bare ice. Due to the method used in extending the one-way simulation, this process is not considered in Le clec'h et al. (2019). Therefore, the comparison of our respective methods for representing the melt–elevation feedback (one-way vs. two-way coupling) lacks a common physical basis.

Another significant aspect of our method under discussion relates to the spatial resolution of the MAR model. To reach a balance between computational efficiency and adequately representing the SMB within the ensemble, we opted for a relatively coarse spatial resolution of 25 km. At the scale of the entire GrIS, this resolution proves to be a viable choice for capturing the global SMB evolution, as supported by previous research (e.g. Fettweis et al., 2020). However, at a finer scale of analysis, this resolution may compromise the accurate representation of local wind and temperature patterns. In some cases, a grid point might span an area as large as the ablation zone, introducing potential inaccuracies (Van de Wal et al., 2012; Hermann et al., 2018). RCMs remain sensitive to horizontal resolution, particularly when aiming to accurately represent SMB and surface energy balance in specific areas. The local representation of processes and surface topography by the model plays a crucial role in this sensitivity (Franco et al., 2012; van de Berg et al., 2020).

5 Conclusions

The coupling of the RCM MAR and the ISM PISM is presented here following the SSP5-8.5 scenario as simulated by CESM2. The two-way coupling is compared to a one-way and a zero-way (uncoupled) experiments to evaluate the importance of the melt–elevation feedback.

The first aim was to study what the GrIS became in 2200 by applying such extreme conditions. Our fully coupled simulation projects a contribution of 64 cm to SLR by 2200 with a stabilised climate since 2100 of $+7\,^{\circ}\mathrm{C}$ compared to our reference period (1961–1990). Until 2100 our results are comparable with results obtained in other studies (e.g. Goelzer et al., 2020).

The most effective approach for representing the melt–elevation feedback involves fully coupling an atmospheric model with an ice sheet model. Neglecting this feedback leads to an underestimation of the projected sea level rise contribution by 10.5 %. When comparing two methods to account for the melt–elevation feedback (coupling and offline correction), we highlight that the corrected SMB from the MAR model underestimates the coupled SMB by 2.5 % when interpolated on the PISM grid using this correction.

The offline correction is no longer valid on the ice sheet margins because it fails to consider the mitigation of temper-

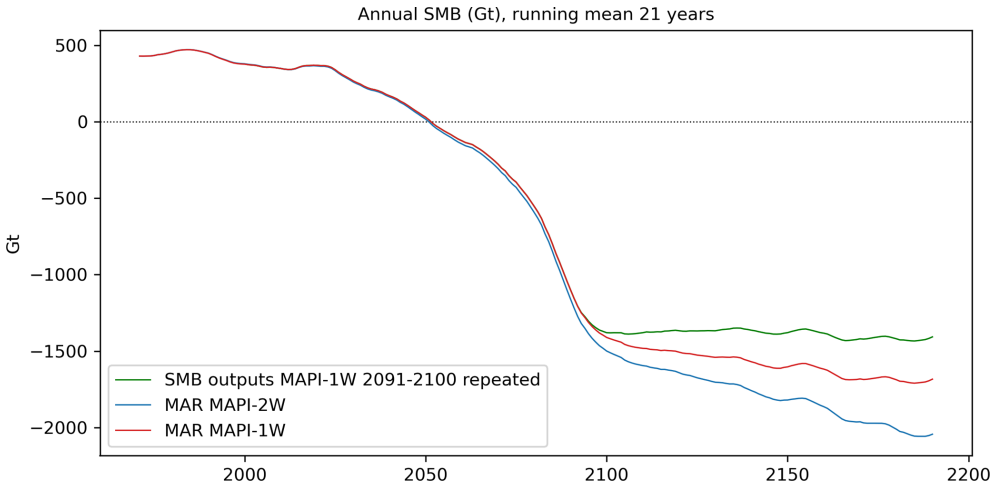

Figure 12. Yearly surface mass balance (SMB) integrated over the entire ice sheet as simulated by uncoupled MAR (no update of the topography, in red); by coupled MAR (topography updated each year, in blue); and by uncoupled MAR until 2100, with the last 10 years of SMB outputs repeated until 2200 (in green).

ature lapse rates, and consequently melt lapse rates, due to changes in topography, such as retreat and slope alterations. These changes influence the wind regime at the margins of the coupled MAR simulation. The mitigation of melt rates depends on the reduction in sensible heat flux due to changes in local wind regimes and temperature lapse rates. A hypothesis to explain these local changes around the ice sheet margins involves modifications of barrier wind regimes. These winds typically act along the ice sheet, transporting warmer air from the tundra, enhancing the surface melt and increasing the northward wind speed along the western side, for instance. The orographic barrier, crucial for the formation of such winds, diminishes with the evolving topography in MAPI-2w. Consequently, enhanced melt could be mitigated, as well as the melt–elevation feedback. However, further investigation is required to validate this assumption and to understand the underlying physical processes responsible for these local wind regime changes initiated by modified surface topography in a warmer climate. A moment budget comparing both simulations (MAPI-1w and MAPI-2w) could help identify differences in local atmospheric circulation patterns leading to such variations in representing melt rates at the margins (van Angelen et al., 2011). Additionally, a complete analysis focusing on characteristics such as recurrence and synoptic situations favourable to the development of these wind events will be necessary to gain a better understanding of the physical processes involved. In conclusion, the coupling is essential to update the surface topography in the RCM and to consider all interactions between the near-surface atmosphere and the new morphology.

By extending our simulations beyond the available period of large-scale forcing of MAR (CESM2), we highlighted that assuming SMB stability when climate conditions become stable is not valid. It is essential to consider the response time of the snowpack to warming rates and its capacity to retain meltwater. Conducting further sensitivity tests will be necessary to determine if the response time of the ice sheet in stabilising the snowpack depends on the parameterisation of snow layer conditions, such as the maximum liquid water content in a layer or the height of the snowpack simulated by the model.

In conclusion, our study emphasises the significance of topography in influencing the local atmospheric pattern, particularly in shaping local wind regimes along the ice sheet margins, in addition to the well-known melt–elevation feedback. Since these processes influence melt in opposite ways, the melt–elevation feedback is mitigated by the evolving topography. This aspect is not accounted for in the commonly used offline correction, which aims to avoid computationally time-consuming coupling between climate and ice sheet models to perform MB projections and to consider the melt–elevation feedback. Neglecting this negative feedback leads to an overestimation of 2.5 % (equivalent to 1.6 cm in 2200) in the SLR contribution compared to the result obtained with full coupling. Such oversight introduces uncertainty in projections (e.g. ISMIP) that fail to consider this process, which can be accurately represented through an atmosphere–dynamics coupling.

Code and data availability. The data used for this study as well as both MAR and PISM models used to generate the data can be found at https://doi.org/10.5281/zenodo.10066184 (Delhasse, 2023).

Supplement. The supplement related to this article is available online at: https://doi.org/10.5194/tc-18-633-2024-supplement.

Author contributions. AD and JB conceived the study. AD and JB performed the simulations. AD led the writing of the manuscript. AD, JB, CK and XF discussed the results. All co-authors revised and contributed to the editing of the manuscript.

Competing interests. At least one of the (co-)authors is a member of the editorial board of *The Cryosphere*. The peer-review process was guided by an independent editor, and the authors also have no other competing interests to declare.

Disclaimer. Publisher's note: Copernicus Publications remains neutral with regard to jurisdictional claims made in the text, published maps, institutional affiliations, or any other geographical representation in this paper. While Copernicus Publications makes every effort to include appropriate place names, the final responsibility lies with the authors.

Acknowledgements. Computational resources used to perform MAR–PISM simulations have been provided by the Consortium des Équipements de Calcul Intensif (CÉCI).

Financial support. This research has been supported by the European Union's Horizon 2020 research and innovation programme (PROTECT; project no. 869304). The Consortium des Équipements de Calcul Intensif (CÉCI) is funded by the F.R.S.–FNRS (grant no. 2.5020.11).

Review statement. This paper was edited by Johannes J. Fürst and reviewed by Maurice Van Tiggelen and one anonymous referee.

References

Agosta, C., Amory, C., Kittel, C., Orsi, A., Favier, V., Gallée, H., van den Broeke, M. R., Lenaerts, J. T. M., van Wessem, J. M., van de Berg, W. J., and Fettweis, X.: Estimation of the Antarctic surface mass balance using the regional climate model MAR (1979–2015) and identification of dominant processes, The Cryosphere, 13, 281–296, https://doi.org/10.5194/tc-13-281-2019, 2019.

Amory, C., Kittel, C., Le Toumelin, L., Agosta, C., Delhasse, A., Favier, V., and Fettweis, X.: Performance of MAR (v3.11) in simulating the drifting-snow climate and surface mass balance of Adélie Land, East Antarctica, Geosci. Model Dev., 14, 3487–3510, https://doi.org/10.5194/gmd-14-3487-2021, 2021.

Aschwanden, A., Bueler, E., Khroulev, C., and Blatter, H.: An enthalpy formulation for glaciers and ice sheets, J. Glaciol., 58, 441–457, https://doi.org/10.3189/2012JoG11J088, 2012.

Aschwanden, A., Aðalgeirsdóttir, G., and Khroulev, C.: Hindcasting to measure ice sheet model sensitivity to initial states, The Cryosphere, 7, 1083–1093, https://doi.org/10.5194/tc-7-1083-2013, 2013.

Aschwanden, A., Fahnestock, M. A., and Truffer, M.: Complex Greenland outlet glacier flow captured, Nat. Commun., 7, 10524, https://doi.org/10.1038/ncomms10524, 2016.

Beckmann, J. and Winkelmann, R.: Effects of extreme melt events on ice flow and sea level rise of the Greenland Ice Sheet, The Cryosphere, 17, 3083–3099, https://doi.org/10.5194/tc-17-3083-2023, 2023.

Bueler, E. and Brown, J.: Shallow shelf approximation as a "sliding law" in a thermomechanically coupled ice sheet model, J. Geophys. Res.-Sol. Ea., 114, 1–21, https://doi.org/10.1029/2008JF001179, 2009.

Choi, Y., Morlighem, M., Rignot, E., and Wood, M.: Ice dynamics will remain a primary driver of Greenland ice sheet mass loss over the next century, Commun. Earth Environ., 2, 1–9, https://doi.org/10.1038/s43247-021-00092-z, 2021.

Delhasse, A.: Main output data used in "Coupling the regional climate MAR model with the ice sheet model PISM mitigates the melt-elevation positive feedback" (Delhasse et al., 2023), Zenodo [data set], https://doi.org/10.5281/zenodo.10066185, 2023.

Delhasse, A., Kittel, C., Amory, C., Hofer, S., van As, D., S. Fausto, R., and Fettweis, X.: Brief communication: Evaluation of the near-surface climate in ERA5 over the Greenland Ice Sheet, The Cryosphere, 14, 957–965, https://doi.org/10.5194/tc-14-957-2020, 2020.

Enderlin, E. M., Howat, I. M., Jeong, S., Noh, M. J., Van Angelen, J. H., and Van Den Broeke, M. R.: An improved mass budget for the Greenland ice sheet, Geophys. Res. Lett., 41, 866–872, https://doi.org/10.1002/2013GL059010, 2014.

Eyring, V., Bony, S., Meehl, G. A., Senior, C. A., Stevens, B., Stouffer, R. J., and Taylor, K. E.: Overview of the Coupled Model Intercomparison Project Phase 6 (CMIP6) experimental design and organization, Geosci. Model Dev., 9, 1937–1958, https://doi.org/10.5194/gmd-9-1937-2016, 2016.

Fettweis, X., Box, J. E., Agosta, C., Amory, C., Kittel, C., Lang, C., van As, D., Machguth, H., and Gallée, H.: Reconstructions of the 1900–2015 Greenland ice sheet surface mass balance using the regional climate MAR model, The Cryosphere, 11, 1015–1033, https://doi.org/10.5194/tc-11-1015-2017, 2017.

Fettweis, X., Hofer, S., Krebs-Kanzow, U., Amory, C., Aoki, T., Berends, C. J., Born, A., Box, J. E., Delhasse, A., Fujita, K., Gierz, P., Goelzer, H., Hanna, E., Hashimoto, A., Huybrechts, P., Kapsch, M.-L., King, M. D., Kittel, C., Lang, C., Langen, P. L., Lenaerts, J. T. M., Liston, G. E., Lohmann, G., Mernild, S. H., Mikolajewicz, U., Modali, K., Mottram, R. H., Niwano, M., Noël, B., Ryan, J. C., Smith, A., Streffing, J., Tedesco, M., van de Berg, W. J., van den Broeke, M., van de Wal, R. S. W., van Kampenhout, L., Wilton, D., Wouters, B., Ziemen, F., and Zolles, T.: GrSMBMIP: intercomparison of the modelled 1980–2012 surface mass balance over the Greenland Ice Sheet, The Cryosphere, 14, 3935–3958, https://doi.org/10.5194/tc-14-3935-2020, 2020.

Fettweis, X., Hofer, S., Séférian, R., Amory, C., Delhasse, A., Doutreloup, S., Kittel, C., Lang, C., Van Bever, J., Veillon, F., and Irvine, P.: Brief communication: Reduction in the future Greenland ice sheet surface melt with the help of solar geoengineering, The Cryosphere, 15, 3013–3019, https://doi.org/10.5194/tc-15-3013-2021, 2021.

Franco, B., Fettweis, X., Lang, C., and Erpicum, M.: Impact of spatial resolution on the modelling of the Greenland ice

sheet surface mass balance between 1990–2010, using the regional climate model MAR, The Cryosphere, 6, 695–711, https://doi.org/10.5194/tc-6-695-2012, 2012.

Goelzer, H., Huybrechts, P., Fürst, J. J., Nick, F. M., Andersen, M. L., Edwards, T. L., Fettweis, X., Payne, A. J., and Shannon, S.: Sensitivity of Greenland ice sheet projections to model formulations, J. Glaciol., 59, 733–749, https://doi.org/10.3189/2013JoG12J182, 2013.

Goelzer, H., Nowicki, S., Payne, A., Larour, E., Seroussi, H., Lipscomb, W. H., Gregory, J., Abe-Ouchi, A., Shepherd, A., Simon, E., Agosta, C., Alexander, P., Aschwanden, A., Barthel, A., Calov, R., Chambers, C., Choi, Y., Cuzzone, J., Dumas, C., Edwards, T., Felikson, D., Fettweis, X., Golledge, N. R., Greve, R., Humbert, A., Huybrechts, P., Le clec'h, S., Lee, V., Leguy, G., Little, C., Lowry, D. P., Morlighem, M., Nias, I., Quiquet, A., Rückamp, M., Schlegel, N.-J., Slater, D. A., Smith, R. S., Straneo, F., Tarasov, L., van de Wal, R., and van den Broeke, M.: The future sea-level contribution of the Greenland ice sheet: a multi-model ensemble study of ISMIP6, The Cryosphere, 14, 3071–3096, https://doi.org/10.5194/tc-14-3071-2020, 2020.

Helsen, M. M., van de Wal, R. S. W., van den Broeke, M. R., van de Berg, W. J., and Oerlemans, J.: Coupling of climate models and ice sheet models by surface mass balance gradients: application to the Greenland Ice Sheet, The Cryosphere, 6, 255–272, https://doi.org/10.5194/tc-6-255-2012, 2012.

Hermann, M., Box, J. E., Fausto, R. S., Colgan, W. T., Langen, P. L., Mottram, R., Wuite, J., Noël, B., van den Broeke, M. R., and van As, D.: Application of PROMICE Q-transect in situ accumulation and ablation measurements (2000–2017) to constrain mass balance at the southern tip of the Greenland Ice Sheet, J. Geophys. Res.-Earth, 123, 1235–1256, 2018.

Hersbach, H., Bell, B., Berrisford, P., Hirahara, S., Horányi, A., Muñoz-Sabater, J., Nicolas, J., Peubey, C., Radu, R., Schepers, D., Simmons, A., Soci, C., Abdalla, S., Abellan, X., Balsamo, G., Bechtold, P., Biavati, G., Bidlot, J., Bonavita, M., De Chiara, G., Dahlgren, P., Dee, D., Diamantakis, M., Dragani, R., Flemming, J., Forbes, R., FUentes, M., Geer, A., Haimberger, L., Healy, S., Hogan, R. J., Hólm, E., Janisková, M., Keeley, S., Laloyaux, P., Lopez, P., Lupu, C., Radnoti, G., De Rosnay, P., Rorum, I., Vamborg, F., Vollaume, S., and Thépaut, J.-N.: The ERA5 global reanalysis, Q. J. Roy. Meteor. Soc., 146, 730, https://doi.org/10.1002/qj.3803, 2020.

Hofer, S., Lang, C., Amory, C., Kittel, C., Delhasse, A., Tedstone, A., and Fettweis, X.: Greater Greenland Ice Sheet contribution to global sea level rise in CMIP6, Nat. Commun., 11, 1–11, https://doi.org/10.1038/s41467-020-20011-8, 2020.

Howat, I., Negrete, A., and Smith, B.: MEaSUREs Greenland Ice Mapping Project (GIMP) Digital Elevation Model from GeoEye and WorldView Imagery, Version 1, NSIDC [data set], https://doi.org/10.5067/H0KUYVF53Q8M, 2017.

Howat, I. M., Negrete, A., and Smith, B. E.: The Greenland Ice Mapping Project (GIMP) land classification and surface elevation data sets, The Cryosphere, 8, 1509–1518, https://doi.org/10.5194/tc-8-1509-2014, 2014.

Johnson, J., Hand, B., and Bocek, T.: Greenland Standard Data Set from SeaRISE master data set for Greenland, Zenodo [data set], https://doi.org/10.5281/zenodo.10637565, 2019.

Joughin, I., Smith, B. E., and Howat, I. M.: A complete map of Greenland ice velocity derived from satellite data collected over 20 years, J. Glaciol., 64, 1–11, https://doi.org/10.1017/jog.2017.73, 2018.

King, M. D., Howat, I. M., Candela, S. G., Noh, M. J., Jeong, S., Noël, B. P., van den Broeke, M. R., Wouters, B., and Negrete, A.: Dynamic ice loss from the Greenland Ice Sheet driven by sustained glacier retreat, Commun. Earth Environ., 1, 1, https://doi.org/10.1038/s43247-020-0001-2, 2020.

Kittel, C., Amory, C., Agosta, C., Jourdain, N. C., Hofer, S., Delhasse, A., Doutreloup, S., Huot, P.-V., Lang, C., Fichefet, T., and Fettweis, X.: Diverging future surface mass balance between the Antarctic ice shelves and grounded ice sheet, The Cryosphere, 15, 1215–1236, https://doi.org/10.5194/tc-15-1215-2021, 2021.

Le clec'h, S., Charbit, S., Quiquet, A., Fettweis, X., Dumas, C., Kageyama, M., Wyard, C., and Ritz, C.: Assessment of the Greenland ice sheet–atmosphere feedbacks for the next century with a regional atmospheric model coupled to an ice sheet model, The Cryosphere, 13, 373–395, https://doi.org/10.5194/tc-13-373-2019, 2019.

Lefebre, F., Gallée, H., van Ypersele, J.-P., and Greuell, W.: Modeling of snow and ice melt at ETH Camp (West Greenland): A study of surface albedo, J. Geophys. Res.-Atmos., 108, D8, https://doi.org/10.1029/2001JD001160, 2003.

Meehl, G. A., Senior, C. A., Eyring, V., Flato, G., Lamarque, J.-F., Stouffer, R. J., Taylor, K. E., and Schlund, M.: Context for interpreting equilibrium climate sensitivity and transient climate response from the CMIP6 Earth system models, Sci. Adv., 6, 1–10, https://doi.org/10.1126/sciadv.aba1981, 2020.

Morlighem, M., Bondzio, J., Seroussi, H., Rignot, E., Larour, E., Humbert, A., and Rebuffi, S.: Modeling of Store Gletscher's calving dynamics, West Greenland, in response to ocean thermal forcing, Geophys. Res. Lett., 43, 2659–2666, 2016.

O'Neill, B. C., Tebaldi, C., van Vuuren, D. P., Eyring, V., Friedlingstein, P., Hurtt, G., Knutti, R., Kriegler, E., Lamarque, J.-F., Lowe, J., Meehl, G. A., Moss, R., Riahi, K., and Sanderson, B. M.: The Scenario Model Intercomparison Project (ScenarioMIP) for CMIP6, Geosci. Model Dev., 9, 3461–3482, https://doi.org/10.5194/gmd-9-3461-2016, 2016.

Oppenheimer, M., Glavovic, B., Hinkel, J., van de Wal, R., Magnan, A., Abd-Elgawad, A., Cai, R., Cifuentes-Jara, M., DeConto, R., Ghosh, T., Hay, J., Isla, F., Marzeion, B., Meyssignac, B., and Z. S.: Sea Level Rise and Implications for Low-Lying Islands, Coasts and Communities, in: IPCC Special Report on the Ocean and Cryosphere in a Changing Climate, edited by: Pörtner, H.-O., Roberts, D., Masson-Delmotte, V., Zhai, P., Tignor, M., Poloczanska, E., Mintenbeck, K., Alegría, A., Nicolai, M., Okem, A., Petzold, J., Rama, B., and Weyer, N., https://doi.org/10.1017/9781009157964.006, 2019.

Quiquet, A., Punge, H. J., Ritz, C., Fettweis, X., Gallée, H., Kageyama, M., Krinner, G., Salas y Mélia, D., and Sjolte, J.: Sensitivity of a Greenland ice sheet model to atmospheric forcing fields, The Cryosphere, 6, 999–1018, https://doi.org/10.5194/tc-6-999-2012, 2012.

Riahi, K., van Vuuren, D. P., Kriegler, E., Edmonds, J., O'Neill, B. C., Fujimori, S., Bauer, N., Calvin, K., Dellink, R., Fricko, O., Lutz, W., Popp, A., Cuaresma, J. C., KC, S., Leimbach, M., Jiang, L., Kram, T., Rao, S., Emmerling, J., Ebi, K., Hasegawa, T., Havlik, P., Humpenöder, F., Da Silva, L. A., Smith, S., Stehfest, E., Bosetti, V., Eom, J., Gernaat, D., Masui, T., Rogelj, J., Strefler, J., Drouet, L., Krey, V., Luderer, G., Harmsen, M.,

Takahashi, K., Baumstark, L., Doelman, J. C., Kainuma, M., Klimont, Z., Marangoni, G., Lotze-Campen, H., Obersteiner, M., Tabeau, A., and Tavoni, M.: The Shared Socioeconomic Pathways and their energy, land use, and greenhouse gas emissions implications: An overview, Global Environ. Chang., 42, 153–168, https://doi.org/10.1016/j.gloenvcha.2016.05.009, 2017.

Robinson, A., Calov, R., and Ganopolski, A.: Greenland ice sheet model parameters constrained using simulations of the Eemian Interglacial, Clim. Past, 7, 381–396, https://doi.org/10.5194/cp-7-381-2011, 2011.

University of Alaska Fairbanks: Parallel Ice Sheet Model, GitHub [code], https://github.com/pism/pism/releases/tag/v1.1.3 (last access: 1 August 2023), 2019.

van Angelen, J. H., Van den Broeke, M., and Van de Berg, W.: Momentum budget of the atmospheric boundary layer over the Greenland ice sheet and its surrounding seas, J. Geophys. Res.-Atmos., 116, D10, https://doi.org/10.1029/2010JD015485, 2011.

van de Berg, W. J., van Meijgaard, E., and van Ulft, L. H.: The added value of high resolution in estimating the surface mass balance in southern Greenland, The Cryosphere, 14, 1809–1827, https://doi.org/10.5194/tc-14-1809-2020, 2020.

van de Wal, R. S. W., Boot, W., Smeets, C. J. P. P., Snellen, H., van den Broeke, M. R., and Oerlemans, J.: Twenty-one years of mass balance observations along the K-transect, West Greenland, Earth Syst. Sci. Data, 4, 31–35, https://doi.org/10.5194/essd-4-31-2012, 2012.

Van den Broeke, M. R. and Gallée, H.: Observation and simulation of barrier winds at the western margin of the Greenland ice sheet, Q. J. Roy. Meteor. Soc., 122, 1365–1383, https://doi.org/10.1256/smsqj.53406, 1996.

Vandecrux, B., Mottram, R., Langen, P. L., Fausto, R. S., Olesen, M., Stevens, C. M., Verjans, V., Leeson, A., Ligtenberg, S., Kuipers Munneke, P., Marchenko, S., van Pelt, W., Meyer, C. R., Simonsen, S. B., Heilig, A., Samimi, S., Marshall, S., Machguth, H., MacFerrin, M., Niwano, M., Miller, O., Voss, C. I., and Box, J. E.: The firn meltwater Retention Model Intercomparison Project (RetMIP): evaluation of nine firn models at four weather station sites on the Greenland ice sheet, The Cryosphere, 14, 3785–3810, https://doi.org/10.5194/tc-14-3785-2020, 2020.

Vizcaíno, M., Mikolajewicz, U., Jungclaus, J., and Schurgers, G.: Climate modification by future ice sheet changes and consequences for ice sheet mass balance, Clim. Dynam., 34, 301–324, https://doi.org/10.1007/s00382-009-0591-y, 2010.

Winkelmann, R., Martin, M. A., Haseloff, M., Albrecht, T., Bueler, E., Khroulev, C., and Levermann, A.: The Potsdam Parallel Ice Sheet Model (PISM-PIK) – Part 1: Model description, The Cryosphere, 5, 715–726, https://doi.org/10.5194/tc-5-715-2011, 2011.

Wyard, C.: Evaluation de la pertinence du couplage entre le modèle de circulation régionale MAR, et le modèle de calotte glaciaire GRISLI, sur le Groenland, Master thesis, Université de Liège, 95 pp., https://hdl.handle.net/2268/172823, 2015.